

MPDATA: A Finite-Difference Solver for Geophysical Flows

Piotr K. Smolarkiewicz^{*,1} and Len G. Margolin^{†,2}

^{*}National Center for Atmospheric Research, Boulder, Colorado 80307; [†]Los Alamos National Laboratory Los Alamos, New Mexico 87545

E-mail: smolar@ncar.ucar.edu, len@lanl.gov

Received March 21, 1997; revised November 11, 1997

This article is a review of MPDATA, a class of methods for the numerical simulation of fluid flows based on the sign-preserving properties of upstream differencing. MPDATA was designed originally as an inexpensive alternative to flux-limited schemes for evaluating the advection of nonnegative thermodynamic variables (such as liquid water or water vapour) in atmospheric models. During the last decade, MPDATA has evolved from a simple advection scheme to a general approach for integrating the conservation laws of geophysical fluids on micro-to-planetary scales. The purpose of this paper is to summarize the basic concepts leading to a family of MPDATA schemes, to review existing MPDATA options, and to demonstrate the use of MPDATA to effectively construct two distinct types of models (elastic and anelastic) for complex geophysical flows. © 1998 Academic Press

Key Words: advection, nonoscillatory approximations, computational fluid dynamics

1. INTRODUCTION

MPDATA (multidimensional positive definite advection transport algorithm [21, 22]) is a finite-difference algorithm for approximating the advective terms in fluid equations. MPDATA is second-order accurate, positive definite,³ conservative, and computationally efficient. It is iterative in nature. The first pass is a simple donor cell approximation, sometimes called upstream differencing, that is positive definite but only first-order accurate. The second pass increases the accuracy of the calculation by estimating and compensating the

¹ The National Center for Atmospheric Research is sponsored by the National Science Foundation.

² Los Alamos National Laboratory is operated by the University of California for the U.S. Department of Energy.

³ Indeed, MPDATA is sign-preserving. However, for historical reasons we shall refer to this property as positive-definiteness or, briefly, positivity.

(second-order) truncation error of the first pass. Additional passes can be used to estimate the residual error of the previous pass and approximately compensate it. This step may be repeated an arbitrary number of times, leading to successively more accurate solutions of the advection equation.

The basic idea [21] is to use the positive definite properties of donor cell schemes to compensate the residual truncation error. Thus MPDATA consists of a sequence of donor cell steps. In the first pass, the velocity is the physical velocity. In the second and subsequent passes, the velocity is calculated from the field that is being advected and has no physical significance. These velocities are termed antidiffusive, or equivalently pseudo velocities.

Originally MPDATA was designed as a simple scheme for handling the transport of non-negative thermodynamic variables (such as liquid water or water vapour) in atmospheric models [21, 22]. In atmospheric modeling, the preservation of sign during numerical advection is the essential aspect of the stability and accuracy in modeling water phase-change or chemical processes [26]. Although advection schemes designed to preserve monotonicity are also positive definite, their use for inhomogeneous transport problems does not suffice to produce monotone solutions [7] and so offers no inherent advantage. Over the years, the theory underlying MPDATA has been extended to advection–diffusion equations and to arbitrary curvilinear frameworks [23], to third-order-accurate approximations [13], as well as to a fully monotone scheme (in the sense of FCT) [24]. More recently, MPDATA has been generalized for systems of equations with arbitrary right-hand sides [25, 28]. The utility of MPDATA as a general solver for complex fluid problems has been demonstrated in the context of atmospheric dynamics for both compressible- and incompressible-type formulations of the equations of motion [28, 31]. MPDATA has also been used as an interpolator [27] in a class of semi-Lagrangian fluid models congruent to the Eulerian MPDATA models [28, 31], as well as a remapper in arbitrary Lagrangian–Eulerian (ALE) simulations of high-speed flows [3, 12]. Several MPDATA-based fluid models have been implemented on massively parallel platforms [1, 2, 16], demonstrating that the local iterative character of the schemes is well-suited to distributed memory architectures.

Generally speaking, MPDATA belongs to the class of nonoscillatory Lax–Wendroff schemes that includes such classical algorithms as FCT [37], TVD [35], and ENO [9]. However, MPDATA is qualitatively different from these other methods, which were developed primarily in the area of high-speed flows to suppress spurious oscillations of Lax–Wendroff schemes for hyperbolic conservation laws. MPDATA was developed for meteorological applications—viz. high Reynolds’ number, low Mach number flows—to reduce the implicit viscosity of the donor cell scheme (commonly used for nonnegative thermodynamic fields in early cloud models) while retaining such virtues as positivity, low phase error, and simplicity of upstream differencing. As a result of its heritage, MPDATA’s focus is on sign preserving multidimensional advection rather than on monotone solutions of hyperbolic conservation laws in one spatial dimension. Unlike TVD and ENO schemes, which employ one-dimensional constructions to limit the scalar flux component, MPDATA effectively limits the magnitude of the vector velocity and so is naturally unsplit. In principle, any of these schemes can be adapted for multidimensional flows of all speeds. However, to our knowledge, MPDATA is the first Lax–Wendroff-type of approach employed consistently (i.e., for all dependent variables) and successfully in geophysical fluid models of all scales.

Over the last decade, MPDATA has been frequently compared with other transport

schemes, primarily in the context of passive scalar advection (see [5, 10, 33] for recent results). The assessments of MPDATA's relative strengths and weaknesses reported in the literature depend very much on the schemes included in comparisons, choice of test problems, MPDATA's options, and details of implementation. The most common complaints are that the basic MPDATA is too diffusive, and enhanced MPDATA is too expensive. The most often acknowledged virtues are MPDATA's multidimensionality, robustness, and its underlying simplicity. These advantages carry over to geophysical fluid models, whereas the relative efficiency of advection becomes less important with increasing complexity of the models [20, 31].

Present geophysical fluid models most often use a centered-in-time-and-space (CTS) approach in their dynamics. To mitigate spurious effects due to negative undershoots in the thermodynamic variables, these models usually adopt a "hybrid" approach where different variables are transported with different advection schemes, or even the same variable uses different advection schemes (operators) in the horizontal and the vertical. Here, the genuine multidimensionality and general applicability of MPDATA allow a single scheme for all dependent variables, thus minimizing auxiliary computations. Furthermore, MPDATA's strong (nonlinear) stability—common to all conservative sign-preserving advection schemes [26]—permits more liberal stopping criteria in iterative elliptic solvers [30] and allows dispensing with various filtering operations often required to stabilize geophysical fluid models. As a result, fluid models based solely on MPDATA appear competitive when compared to established codes of the same category [20, 31].

Since its origin in the early eighties, MPDATA has evolved from a simple advection scheme to a general approach for integrating the conservation laws of geophysical fluids on micro-to-planetary scales. In consequence, MPDATA embodies a family of schemes of varying accuracy and levels of complexity. The MPDATA literature is quite extensive, and continuously expanding on the finer issues of finite-difference transport [13, 18]. The purpose of this paper is twofold. Specifically, we offer to the interested reader an organized tour through numerous topics discussed in the MPDATA literature. For this, we summarize basic concepts underlying the design of MPDATA schemes and review the existing options. More generally, we identify and assemble elements important for designing geophysical fluid models. We start with elementary advection and finish with two diverse examples from modeling geophysical flows. These examples are selected purposely from the areas dominated traditionally by CTS methods; they do not require (but do benefit from) positivity of the advection schemes. Consequently, they do not emphasize the obvious advantages of MPDATA—there are already many such examples in the literature—but rather illustrate how to put the entire approach to work and, in more general terms, document that modern nonoscillatory Lax–Wendroff type schemes offer a viable alternative to the traditional methods for geophysical flows.

The paper is organized as follows. In order to introduce the philosophy of MPDATA schemes we focus in Section 2.1 on the elementary problem of one-dimensional transport of a scalar field in a predetermined uniform flow. In Section 2.2, we extend the basic MPDATA to two-dimensional flows. In Section 2 we also address the stability and convergence of the basic schemes. In Section 3, we posit a model prognostic equation for fluids to derive a general form of the MPDATA algorithm. Then we review various MPDATA options accommodating particular needs of different fluid models. In Section 4, we conclude the paper with examples of elastic and anelastic type fluid models built solely on MPDATA schemes.

2. BASIC MPDATA

2.1. One-Dimensional Advection

The model advection equation for a scalar variable Ψ in one dimension is

$$\frac{\partial \Psi}{\partial t} = -\frac{\partial}{\partial x}(u\Psi), \quad (1)$$

where the velocity u may vary in space and time. The donor cell (or upstream) approximation to the advection equation (1) is written in flux form,

$$\Psi_i^{n+1} = \Psi_i^n - [F(\Psi_i^n, \Psi_{i+1}^n, U_{i+1/2}) - F(\Psi_{i-1}^n, \Psi_i^n, U_{i-1/2})], \quad (2)$$

where the flux function F is defined in terms of the local Courant number U by

$$F(\Psi_L, \Psi_R, U) \equiv [U]^+ \Psi_L + [U]^- \Psi_R \quad (3a)$$

$$U \equiv \frac{u\delta t}{\delta x}, \quad [U]^+ \equiv 0.5(U + |U|), \quad [U]^- \equiv 0.5(U - |U|). \quad (3b), (3c), (3d)$$

The integer and half integer indices correspond to the cell centers and cell walls, respectively. Here δt is the computational time step, δx is the length of a cell, and $[U]^+$ and $[U]^-$ are the nonnegative and nonpositive parts of the Courant number, respectively.

Assume for simplicity that the velocity is constant and Ψ nonnegative (cf. Section 3). A simple truncation analysis, expanding about the time level n and spatial point i , shows that (2) more accurately approximates the advection–diffusion equation

$$\frac{\partial \Psi}{\partial t} = -\frac{\partial}{\partial x}(u\Psi) + \frac{\partial}{\partial x} \left(K \frac{\partial \Psi}{\partial x} \right), \quad (4)$$

where

$$K = \frac{(\delta x)^2}{2\delta t} (|U| - U^2). \quad (5)$$

Thus (2) approximates the solution to the advection equation with a second-order error. To improve the accuracy, it is necessary to construct a numerical estimate of the error and subtract it from (2). The classical one-step Lax–Wendroff scheme is perhaps the most familiar example of such a procedure, using standard centered differences to approximate the second term on RHS of (4). While MPDATA derives from the same general concept, it exploits special properties of the donor cell scheme for approximating and compensating the error.

The donor cell scheme (2) is positive definite for any velocity field and is monotone if the velocity field is constant in space, providing that the Courant number is properly bounded. These properties are lost in any linear combination of donor cell and centered differencing [6]. In these terms, the basic idea underlying all MPDATA schemes can be stated very simply—use a donor cell approximation to the error term. Since the error term is not written in a form to do this directly, it is first rewritten as

$$\text{error}^{(1)} = \frac{\partial}{\partial x} (v^{(1)}\Psi), \quad (6)$$

where

$$v^{(1)} \equiv \frac{(\delta x)^2}{2\delta t} (|U| - U^2) \frac{1}{\Psi} \frac{\partial \Psi}{\partial x} \quad (7)$$

is a pseudo velocity. The superscript ⁽¹⁾ shows that it is the first approximation to subtracting the error. Inside the derivative in (6), the diffusive flux in the second term of (4) is multiplied by a factor of Ψ over Ψ —i.e., by unity. However, in the donor cell approximation to (6), the factor in the numerator will be represented using an upstream value, whereas the factor in the denominator will be approximated using a centered value. In this way, a nonlinearity is introduced and a higher-order approximation is found that still preserves positivity.

To compensate for the error between the donor cell solution $\Psi^{(1)}$ and a second-order accurate solution Ψ^{n+1} , we use the error (6) estimated at time level $n + 1$. A first-order accurate estimate of the pseudo velocity (nondimensionalized for convenience) is

$$V_{i+1/2}^{(1)} \equiv (|U| - U^2) \frac{\Psi_{i+1}^{(1)} - \Psi_i^{(1)}}{\Psi_{i+1}^{(1)} + \Psi_i^{(1)}} \equiv (|U| - U^2) A_{i+1/2}^{(1)}, \quad (8)$$

where

$$V^{(1)} = \frac{v^{(1)} \delta t}{\delta x}. \quad (9)$$

In the second pass, we subtract a donor cell estimate of the error to improve the order of the approximation. The equation of the second pass is

$$\Psi_i^{(2)} = \Psi_i^{(1)} - [F(\Psi_i^{(1)}, \Psi_{i+1}^{(1)}, V_{i+1/2}^{(1)}) - F(\Psi_{i-1}^{(1)}, \Psi_i^{(1)}, V_{i-1/2}^{(1)})], \quad (10)$$

which estimates Ψ^{n+1} to the second-order while preserving the sign of Ψ . Note that the stability of the first pass ensures that of the second pass, since $|U| \leq 1 \implies -1 \leq |U| - U^2 \leq 1$ and the assumed nonnegativity of Ψ , together with the positivity of the donor-cell scheme assure $|A_{i+1/2}^{(1)}| \leq 1 \forall i$. For illustration, Table 1 summarizes a series of elementary advection tests (uniform translation of a Gaussian pulse) for a range of spatial resolutions and Courant numbers. The numbers displayed are the logarithm base 2 of the global truncation error (evaluated as the rms error between corresponding numerical and analytic solutions; [13, 24]) that evidence the second-order convergence of the scheme.

TABLE 1

Logarithms Base 2 of the Global Truncation Error for a Series of Simulations Using Basic MPDATA Where a Gaussian Pulse Is Advected over a Fixed Distance by a Constant Flow

	$U = 0.05$	$U = 0.35$	$U = 0.65$	$U = 0.95$
$\delta x = 2^0 \delta x_0$	-9.86	-10.5	-11.3	-13.9
$\delta x = 2^{-1} \delta x_0$	-11.6	-12.4	-13.3	-15.8
$\delta x = 2^{-2} \delta x_0$	-13.6	-14.4	-15.3	-17.8
$\delta x = 2^{-3} \delta x_0$	-15.5	-16.4	-17.3	-19.8
$\delta x = 2^{-4} \delta x_0$	-17.5	-18.4	-19.3	-21.8
$\delta x = 2^{-5} \delta x_0$	-19.5	-20.4	-21.3	-23.8
$\delta x = 2^{-6} \delta x_0$	-21.5	-22.4	-23.3	-25.8
$\delta x = 2^{-7} \delta x_0$	-23.5	-24.4	-25.3	-27.8

The two-pass scheme described above is the most elementary MPDATA. Equation (10) again can be expanded in a Taylor series, the residual error after the second pass estimated as in (6)–(8), and compensated as in (10). The entire process of estimating the residual error and compensating it can be continued, iteration after iteration, reducing the magnitude of the truncation error which remains at third-order [13]. It is worth noting that writing a computer program for such a procedure is extremely simple, as the flux function, the donor cell scheme itself, and the form of the pseudo velocity remain the same in each iteration.

2.2. Extension to Two Dimensions

The extension of the scheme from one to two dimensions contains a subtlety originating in the cross derivatives that appear in the truncation analysis. However, the extension from two dimensions to an arbitrary M is straightforward (see Section 3.2), and for simplicity we describe only the two-dimensional case. We assume a regular staggered mesh with the field Ψ stored at the cell centers (denoted by integer indices) and the velocity components stored at the cell edges (denoted by one half-integer index and one integer index) such that the x -component u is stored at $[(i + 1/2)\delta x, j\delta y]$ edges, whereas the y -component v is stored at $[i\delta x, (j + 1/2)\delta y]$ edges.

The numerical equation for donor cell advection in two dimensions can be written

$$\Psi_{i,j}^{n+1} = \Psi_{i,j}^n - [F(\Psi_{i,j}^n, \Psi_{i+1,j}^n, U_{i+1/2,j}) - F(\Psi_{i-1,j}^n, \Psi_{i,j}^n, U_{i-1/2,j})] - [F(\Psi_{i,j}^n, \Psi_{i,j+1}^n, V_{i,j+1/2}) - F(\Psi_{i,j-1}^n, \Psi_{i,j}^n, V_{i,j-1/2})], \tag{11}$$

where now U and V are the dimensionless Courant numbers

$$U \equiv \frac{u\delta t}{\delta x}, \quad V \equiv \frac{v\delta t}{\delta y} \tag{12}$$

and the flux function F has been defined in (3).

Still assuming constant velocities, we expand (11) about the cell center (i, j) and time level n . The result is an advection–diffusion equation

$$\frac{\partial \Psi}{\partial t} = -\frac{\partial}{\partial x}(u\Psi) - \frac{\partial}{\partial y}(v\Psi) + \frac{|U|(\delta x)^2}{2\delta t}(1 - |U|)\frac{\partial^2 \Psi}{\partial x^2} + \frac{|V|(\delta y)^2}{2\delta t}(1 - |V|)\frac{\partial^2 \Psi}{\partial y^2} - \frac{UV\delta x\delta y}{\delta t}\frac{\partial^2 \Psi}{\partial x\partial y}. \tag{13}$$

The idea is now to write a donor cell estimate of the truncation error and subtract it from the difference equation (11) to create a higher-order approximation. Note that when we write this in a form using pseudo velocities, the cross-term gives us a degree of freedom not present in the one-dimensional analysis. That is, writing (13) as

$$\frac{\partial \Psi}{\partial t} = -\frac{\partial}{\partial x}(u\Psi) - \frac{\partial}{\partial y}(v\Psi) + \frac{\partial}{\partial x}(u^{(1)}\Psi) + \frac{\partial}{\partial y}(v^{(1)}\Psi) \tag{14}$$

we can choose

$$u^{(1)} = \frac{|U|(\delta x)^2}{2\delta t}(1 - |U|)\frac{1}{\Psi}\frac{\partial \Psi}{\partial x} - f\frac{UV\delta x\delta y}{\delta t}\frac{1}{\Psi}\frac{\partial \Psi}{\partial y}, \tag{15a}$$

$$v^{(1)} = \frac{|V|(\delta y)^2}{2\delta t}(1 - |V|)\frac{1}{\Psi}\frac{\partial \Psi}{\partial y} - (1 - f)\frac{UV\delta x\delta y}{\delta t}\frac{1}{\Psi}\frac{\partial \Psi}{\partial x}, \tag{15b}$$

where the real number f is arbitrary. This extra freedom is useful when deriving some more advanced options of MPDATA [13]. In a practical sense, the implementation of (15) is insensitive to the choice of f (at least in the range $0 \leq f \leq 1$), and $f = 0.5$ is used as a default in all MPDATA schemes.

The pseudo velocities (15) must be evaluated at the cell edges. Their explicit form will depend upon whether the edge is horizontal or vertical. In either case we can write in dimensionless form,

$$U^{(1)} \equiv \frac{u^{(1)}\delta t}{\delta x} = |U|(1 - |U|)A^{(1)} - 2fUVB^{(1)}, \quad (16a)$$

$$V^{(1)} \equiv \frac{v^{(1)}\delta t}{\delta y} = |V|(1 - |V|)B^{(1)} - 2(1 - f)UVA^{(1)}, \quad (16b)$$

where $A^{(1)}$ and $B^{(1)}$ are numerical estimates at the particular edge. For example, on the right edge of a cell

$$A^{(1)} \equiv \left[\frac{\delta x}{2\Psi} \frac{\partial \Psi}{\partial x} \right]_{i+1/2,j}^{n+1} = \frac{\Psi_{i+1,j}^{(1)} - \Psi_{i,j}^{(1)}}{\Psi_{i+1,j}^{(1)} + \Psi_{i,j}^{(1)}}, \quad (17a)$$

$$B^{(1)} \equiv \left[\frac{\delta y}{2\Psi} \frac{\partial \Psi}{\partial y} \right]_{i+1/2,j}^{n+1} = \frac{1}{2} \frac{\Psi_{i+1,j+1}^{(1)} + \Psi_{i,j+1}^{(1)} - \Psi_{i+1,j-1}^{(1)} - \Psi_{i,j-1}^{(1)}}{\Psi_{i+1,j+1}^{(1)} + \Psi_{i,j+1}^{(1)} + \Psi_{i+1,j-1}^{(1)} + \Psi_{i,j-1}^{(1)}}, \quad (17b)$$

where $\Psi^{(1)}$ is the solution after the first donor cell pass. Other approximations to A and B are also possible. Those in (17) have the virtue of proper boundedness (given the stability and positive definiteness of the original donor cell scheme) that is important for the stability of the multidimensional MPDATA [22]. The equation of the second pass is

$$\begin{aligned} \Psi_{i,j}^{(2)} = & \Psi_{i,j}^{(1)} - [F(\Psi_{i,j}^{(1)}, \Psi_{i+1,j}^{(1)}, U_{i+1/2,j}^{(1)}) - F(\Psi_{i-1,j}^{(1)}, \Psi_{i,j}^{(1)}, U_{i-1/2,j}^{(1)})] \\ & - [F(\Psi_{i,j}^{(1)}, \Psi_{i,j+1}^{(1)}, V_{i,j+1/2}^{(1)}) - F(\Psi_{i,j-1}^{(1)}, \Psi_{i,j}^{(1)}, V_{i,j-1/2}^{(1)})], \end{aligned} \quad (18)$$

and the resulting two-pass scheme already offers second-order accuracy. Continuing iterations further reduce the amplitude of the leading third-order error (see [13] and/or [22] for comparisons of the results using different numbers of iterations).

As in the 1D case, the stability of the first pass controls the stability of subsequent iterations and, therefore, the stability of multidimensional MPDATA. The original proof of stability has been given in Section 3 of [22]. It follows that limiting the maximal sum of absolute values of local partial Courant numbers to not exceed 0.5 (here, $|U| + |V| \leq 0.5$) is a sufficient condition for both the stability and positivity of a multipass MPDATA in $M \leq 3$ spatial dimensions for an arbitrary velocity field. Furthermore, positivity and global conservation assure the solution boundedness in the L_2 norm, which is equivalent to the nonlinear stability statement [26]. Limiting the sum of local partial Courant numbers by 0.5 is the result of assuming (in the proof) a worst case scenario where the velocity components flip their signs across the cell (see discussions in Section 2 of [22] and Section 6.1 of [13]). In CFD applications, this rarely happens, and the heuristic limit we use for advection—in

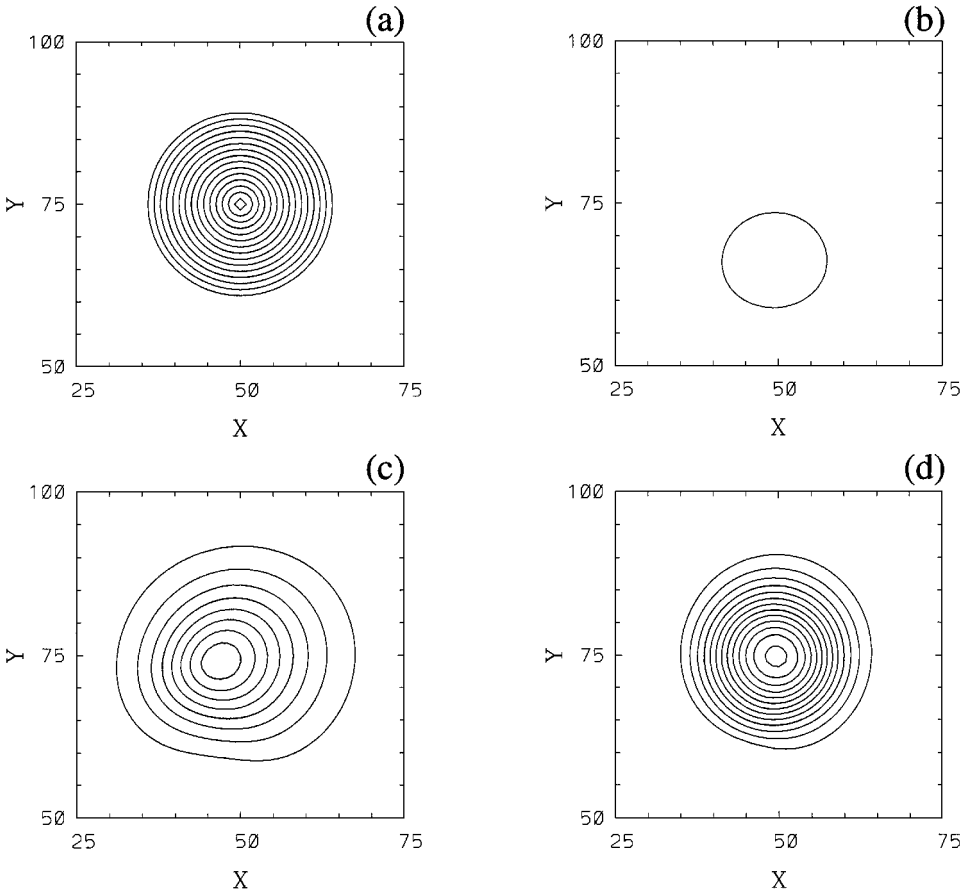


FIG. 1. Isolines of a cone advected through six full rotations (3768 timesteps) using different variants of MPDATA. The contour interval is 0.25, and the zero contour line is not shown. Plate(a) shows the analytic solution (identical to the initial condition), plate(b) shows the result using the classical donor cell scheme, plate(c) shows the basic MPDATA scheme, and plate (d) shows the most accurate MPDATA option discussed in Section 3.

fact, in all MPDATA extensions—is 1.0, i.e., the standard condition for the stability of the donor cell scheme (cf. Eq. (3-140) of Roache [17]).

For illustration, Fig. 1 displays the results of a standard solid-body rotation test (cf. [37, 13, 21–24]) using selected variants of MPDATA. The two-dimensional rotation test employs a square mesh of 101 by 101 points. The angular velocity $\omega = 0.1$ and the velocity components are $(u, v) = -\omega(y - y_0, x - x_0)$. The center of rotation (x_0, y_0) is the center of the mesh $(50\delta x, 50\delta y)$. The maximum Courant number $(|U| + |V|)$ is 0.99, and one full rotation requires 628 time steps. The initial condition is a cone centered at the point $(75\delta x, 50\delta y)$ and has a base diameter of 30 and a height of 4. Figures 1a–c show the analytic solution, the first-order donor cell solution, and the second-order solution using basic two-pass MPDATA, all after six rotations (more qualitative displays in a 3D perspective are available in, respectively, Figs. 1 and 2 of [21], 8 of [22], and 1b of [27], where comparisons with other solutions are also presented). Figure 1d anticipates the discussion of the next section and displays the state-of-the-art third-order accurate two-pass MPDATA option with the analytic summation of the infinite series of corrective iterations [13]. The schemes in

Figs. 1c and 1d use approximately 2.5 and 6 times as much computer time as the donor cell algorithm.

3. REVIEW OF MPDATA OPTIONS

3.1. A Prototype Fluid Problem

Before presenting some available MPDATA options, it is instructional to introduce a generalized transport equation,

$$\frac{\partial G\Psi}{\partial t} + \nabla \cdot (\mathbf{v}\Psi) = GR, \quad (19)$$

where $G = G(\mathbf{x})$, $\mathbf{v} = \mathbf{v}(\mathbf{x}, t)$, and $R = R(\mathbf{x}, t)$ are assumed to be known functions. In fluid dynamics applications, G may play the role of the Jacobian of the coordinate transformation from the Cartesian \mathbf{x}_C to the curvilinear framework \mathbf{x} ,⁴ \mathbf{v} may be viewed as a generalized “advective” velocity vector $\mathbf{v} = G\dot{\mathbf{x}}$, and R may combine all forcings and/or sources. Then both \mathbf{v} and R are functionals of the dependent variables rather than functions of the independent variables (see Section 4 for examples).

In order to design a fully second-order MPDATA scheme for (19), we shall extend the procedure discussed in Section 2 while following the development in [25, 28]. We assume a temporal discretization of (19) in the form

$$\frac{G\Psi^{n+1} - G\Psi^n}{\delta t} + \nabla \cdot (\mathbf{v}^{n+1/2}\Psi^n) = GR^{n+1/2}. \quad (20)$$

Expanding (20) into a second-order Taylor series about $t = n\delta t$ gives

$$G \frac{\partial \Psi}{\partial t} + \frac{1}{2} \delta t G \frac{\partial^2 \Psi}{\partial t^2} + \nabla \cdot \left[\left(\mathbf{v} + \frac{1}{2} \delta t \frac{\partial \mathbf{v}}{\partial t} \right) \Psi \right] = GR + \frac{1}{2} \delta t G \frac{\partial R}{\partial t} + \mathcal{O}(\delta t^2). \quad (21)$$

To convert temporal derivatives into spatial derivatives, we take $(\partial/\partial t)$ (21), resulting in

$$G \frac{\partial^2 \Psi}{\partial t^2} + \nabla \cdot \left(\frac{\partial \mathbf{v}}{\partial t} \Psi + \mathbf{v} \frac{\partial \Psi}{\partial t} \right) = G \frac{\partial R}{\partial t} + \mathcal{O}(\delta t). \quad (22)$$

Since (21) implies

$$\frac{\partial \Psi}{\partial t} = -\frac{1}{G} \nabla \cdot (\mathbf{v}\Psi) + R + \mathcal{O}(\delta t), \quad (23)$$

(22) may be rewritten as

$$G \frac{\partial^2 \Psi}{\partial t^2} = \nabla \cdot \left[-\frac{\partial \mathbf{v}}{\partial t} \Psi + \frac{1}{G} \mathbf{v}(\mathbf{v} \cdot \nabla \Psi) + \frac{1}{G} \mathbf{v}\Psi(\nabla \cdot \mathbf{v}) - \mathbf{v}R \right] + G \frac{\partial R}{\partial t} + \mathcal{O}(\delta t). \quad (24)$$

Inserting (24) in (21) and regrouping the terms that do not cancel leads finally to the modified

⁴ In some instances (e.g., for the anelastic type fluid models), G may be a product of the Jacobian and the fluid density (see Section 4 for examples).

equation

$$\begin{aligned} \frac{\partial G\Psi}{\partial t} + \nabla \cdot (\mathbf{v}\Psi) = GR - \nabla \cdot \left[\frac{1}{2}\delta t \frac{1}{G} \mathbf{v}(\mathbf{v} \cdot \nabla \Psi) + \frac{1}{2}\delta t \frac{1}{G} \mathbf{v}\Psi(\nabla \cdot \mathbf{v}) \right] \\ + \nabla \cdot \left(\frac{1}{2}\delta t \mathbf{v}R \right) + \mathcal{O}(\delta t^2), \end{aligned} \quad (25)$$

where all $\mathcal{O}(\delta t)$ errors due to the uncentered time differencing in (20) are now expressed by spatial derivatives. Note that assuming the time levels of both the advective velocity and forcing term are $n + 1/2$ in (20) eliminates $\mathcal{O}(\delta t)$ truncation errors proportional to their temporal derivatives in (25). Any $\mathcal{O}(\delta t^2)$ approximations to $\mathbf{v}^{n+1/2}$ and $R^{n+1/2}$ would suffice for second-order accuracy in (20); particular approximations will be discussed in Section 3.4. Note also that for a 2D problem with $R \equiv G - 1 \equiv 0$ and constant \mathbf{v} , (25) is equivalent to (13) except for the terms $\sim \delta x |u| (\partial^2 \Psi / \partial x^2)$ and $\sim \delta y |v| (\partial^2 \Psi / \partial y^2)$ present in (13) that derive from upwind spatial differences in the donor cell scheme. These terms do not involve conversion from the temporal to spatial derivatives.

The $\mathcal{O}(\delta t)$ truncation errors on the RHS of (25) have two distinct components. The first is solely due to advection and depends linearly on Ψ . The second is solely due to the forcing and its dependence on Ψ is, in general, unknown. In the following section we present elementary MPDATA options for homogeneous transport, while in Section 3.3 we describe how to compensate the errors due to the nonvanishing forcing. Section 3.4 elaborates on several approximations to advective velocities. Section 3.5 briefly introduces other MPDATA options.

3.2. MPDATA Options for Homogeneous Transport

(1) *Introductory remarks.* With $R \equiv 0$ in (19) all MPDATA schemes retain the form of the basic scheme (Section 2), where all subsequent iterations are standard donor cell scheme but with different arguments at each iteration. The first iteration uses the advective velocity $\mathbf{v}^{n+1/2}$ and Ψ^n , whereas following iterations use pseudo velocities and Ψ evaluated from the preceding iterations. This is compactly written as

$$\Psi_{\mathbf{i}}^{(k)} = \Psi_{\mathbf{i}}^{(k-1)} - \frac{1}{G_{\mathbf{i}}} \sum_{I=1}^M \left[F\left(\Psi_{\mathbf{i}}^{(k-1)}, \Psi_{\mathbf{i}+\mathbf{e}_I}^{(k-1)}, V_{\mathbf{i}+1/2\mathbf{e}_I}^{I(k)}\right) - F\left(\Psi_{\mathbf{i}-\mathbf{e}_I}^{(k-1)}, \Psi_{\mathbf{i}}^{(k-1)}, V_{\mathbf{i}-1/2\mathbf{e}_I}^{I(k)}\right) \right], \quad (26)$$

where $\mathbf{i} \equiv (i^1, \dots, i^M)$ denotes a location on the M -dimensional regular grid; \mathbf{e}_I is the unit vector in the I th of M spatial directions; F is the donor cell flux function defined in (3) with V^I denoting the normalized advective pseudo velocity in I th direction; integer and half integer indices correspond to the cell centers and edges, respectively; and $k = 1, \dots, IORD$ numbers MPDATA iterations such that

$$\Psi^{(0)} \equiv \Psi^n, \quad \Psi^{(IORD)} \equiv \Psi^{n+1} \quad (27a), (27b)$$

$$V^{I(k+1)} = V^I(\mathbf{V}^{(k)}, \Psi^{(k)}, G), \quad V_{\mathbf{i}+1/2\mathbf{e}_I}^{I(1)} \equiv u^I \Big|_{\mathbf{i}+1/2\mathbf{e}_I} \frac{\delta t}{\delta x^I}. \quad (28a), (28b)$$

With this notation (originated in [22]), $IORD = 1$ variant of MPDATA is the classical donor cell scheme, and various options of MPDATA differ merely by specifics of the functional form of the pseudo velocity (28a).

(2) *Solenoidal flows* ($\nabla \cdot \mathbf{v} = 0$). For solenoidal flows (e.g., incompressible or anelastic fluid models) the standard representation of (28a) takes the form

$$\begin{aligned}
 V_{\mathbf{i}+1/2\mathbf{e}_l}^{I(k+1)} = & \left[|V_{\mathbf{i}+1/2\mathbf{e}_l}^{I(k)}| - \frac{\left(V_{\mathbf{i}+1/2\mathbf{e}_l}^{J(k)}\right)^2}{0.5(G_{\mathbf{i}+\mathbf{e}_l} + G_{\mathbf{i}})} \right] \frac{\Psi_{\mathbf{i}+\mathbf{e}_l}^{(k)} - \Psi_{\mathbf{i}}^{(k)}}{\Psi_{\mathbf{i}+\mathbf{e}_l}^{(k)} + \Psi_{\mathbf{i}}^{(k)}} \\
 & - \sum_{J=1; J \neq I}^M \frac{V_{\mathbf{i}+1/2\mathbf{e}_l}^{I(k)} \overline{V_{\mathbf{i}+1/2\mathbf{e}_l}^{J(k)}}}{(G_{\mathbf{i}+\mathbf{e}_l} + G_{\mathbf{i}})} \\
 & \times \frac{\Psi_{\mathbf{i}+\mathbf{e}_l+\mathbf{e}_j}^{(k)} + \Psi_{\mathbf{i}+\mathbf{e}_l}^{(k)} - \Psi_{\mathbf{i}+\mathbf{e}_l-\mathbf{e}_j}^{(k)} - \Psi_{\mathbf{i}-\mathbf{e}_j}^{(k)}}{\Psi_{\mathbf{i}+\mathbf{e}_l+\mathbf{e}_j}^{(k)} + \Psi_{\mathbf{i}+\mathbf{e}_l}^{(k)} + \Psi_{\mathbf{i}+\mathbf{e}_l-\mathbf{e}_j}^{(k)} + \Psi_{\mathbf{i}-\mathbf{e}_j}^{(k)}}
 \end{aligned} \quad (29a)$$

where

$$\overline{V_{\mathbf{i}+1/2\mathbf{e}_l}^{J(k)}} \equiv \frac{1}{4} \left(V_{\mathbf{i}+\mathbf{e}_l+1/2\mathbf{e}_j}^{J(k)} + V_{\mathbf{i}+1/2\mathbf{e}_l}^{J(k)} + V_{\mathbf{i}+\mathbf{e}_l-1/2\mathbf{e}_j}^{J(k)} + V_{\mathbf{i}-1/2\mathbf{e}_l}^{J(k)} \right). \quad (29b)$$

Equations (29) are finite difference representations of the expression under the divergence operator in the second term on the RHS of (25) normalized by Ψ , plus the pseudo velocity component (proportional to the absolute value of V) accounting for the truncation errors due to the upwind spatial differencing (3) in (26). By design, the resulting scheme (26)–(29) is fully second-order accurate (while sign preserving) for a smooth solenoidal flow $\mathbf{v}(\mathbf{x}, t)$ and stationary function $G(\mathbf{x})$, given properly bounded local Courant numbers $G^{-1}\mathbf{V}^{(1)}$ (cf. the discussion following (18) in Section 2.2 of this paper, and note that the advective velocity itself is proportional to G).

(3) *Divergent flows* ($\nabla \cdot \mathbf{v} \neq 0$). For divergent flows (e.g., compressible or elastic fluid models; or anelastic models with the alternate-direction implementation of MPDATA) the truncation error term proportional to flow divergence on the RHS of (25) becomes significant. Since the character of the model rarely changes in the course of simulation,⁵ we incorporate the compensation of this error as a special option (rather than a default) into MPDATA programs. Such an optional extension of (29) may be written, for example, as

$$\begin{aligned}
 V_{\mathbf{i}+1/2\mathbf{e}_l}^{I(k+1)} = & \dots - \frac{1}{2} \frac{V_{\mathbf{i}+1/2\mathbf{e}_l}^{I(k)}}{(G_{\mathbf{i}+\mathbf{e}_l} + G_{\mathbf{i}})} \left(V_{\mathbf{i}+3/2\mathbf{e}_l}^{I(k)} - V_{\mathbf{i}-1/2\mathbf{e}_l}^{I(k)} \right) \\
 & - \frac{1}{2} \frac{V_{\mathbf{i}+1/2\mathbf{e}_l}^{I(k)}}{(G_{\mathbf{i}+\mathbf{e}_l} + G_{\mathbf{i}})} \sum_{J=1; J \neq I}^M \left(V_{\mathbf{i}+\mathbf{e}_l+1/2\mathbf{e}_j}^{J(k)} + V_{\mathbf{i}+1/2\mathbf{e}_l}^{J(k)} - V_{\mathbf{i}+\mathbf{e}_l-1/2\mathbf{e}_j}^{J(k)} - V_{\mathbf{i}-1/2\mathbf{e}_l}^{J(k)} \right),
 \end{aligned} \quad (30)$$

where the omitted terms are those in (29). This correction is insignificant in solenoidal flows even though the pseudo velocities are in general divergent (Section 5.1 in [22]). Although the expression in (30) might be written in a more compact form, we purposely retain (here as well as in other formulas) the form resembling our actual FORTRAN coding.

(4) *Transporting fields of variable sign*. So far, we have assumed that the transported field Ψ is exclusively either nonnegative or nonpositive. This assumption is important for

⁵ Switching from compressible to incompressible model formulation may occur, e.g., in time-dependent geometry [15].

the stability, accuracy, and, generally speaking, for the design of MPDATA. However, it enters MPDATA schemes explicitly only in the pseudo velocity formulae, in the A and B terms $\sim \Delta \Psi / \sum \Psi$ of the finite difference approximations to the $(1/\Psi)(\partial \Psi / \partial x^I)$ ratios—cf. (8), (17), and (29). Note that these terms are bounded when Ψ is of a constant sign. When Ψ changes sign, $|A|$ and $|B|$ are unbounded leading to arbitrarily large pseudo velocities and unstable schemes. MPDATA can be extended to transport of variable-sign fields in a number of ways. Below we outline a few that have proven useful in applications.

The simplest and most common way is to replace all Ψ s in (8), (17), and (29) with $|\Psi|$ s. This exploits the relationship

$$\frac{1}{\Psi} \frac{\partial \Psi}{\partial x^I} \equiv \frac{1}{2\mu} \frac{1}{(\Psi^2)^\mu} \frac{\partial (\Psi^2)^\mu}{\partial x^I} \Bigg|_{\mu=1/2} = \frac{1}{|\Psi|} \frac{\partial |\Psi|}{\partial x^I}. \quad 6$$

The results are, practically, insensitive to the value of μ ; however $\mu = 1/2$ is the optimal choice as it merely requires replacing Ψ with $|\Psi|$ in the pseudo velocity formulae derived for the constant-sign fields and is computationally the most efficient.

An alternate approach exploits the mass continuity equation (Section 4 in [23]). Multiplying Eq. (19)—with $\Psi = \chi$ being the fluid density (elastic systems), or with $\Psi = \chi \equiv 1$ and a steady reference density included in G (anelastic systems); see Section 4—by an arbitrary constant c and adding the resulting equation to (19) leads to

$$\frac{\partial G(\Psi + c\chi)}{\partial t} + \nabla \cdot (\mathbf{v}(\Psi + c\chi)) = GR. \quad (31)$$

This illustrates another class of degrees of freedom in MPDATA. First, the arbitrary constant c can be chosen to assure positivity of Ψ^n [23, 13]. Second, it makes MPDATA susceptible to asymptotic linear analysis as $c \nearrow \infty$ [23]. Third, MPDATA itself can be linearized around an arbitrary large constant leading straightforwardly to a two-pass scheme that differs technically from the basic algorithm only in two details: at the second iteration, the donor cell flux function in (26) takes the value unity in its first two arguments, and the pseudo velocities in (29) replace each Ψ with unity in the two “ $\sum \Psi$ ” denominators. This asymptotic form of MPDATA is a realization of the classical Lax–Wendroff algorithm (cf. Section 4 in [23]). Combined with a nonoscillatory enhancement (Section 3.5.3) it makes a viable scheme for transporting momenta in fluid models (see Section 4 for examples).

3.3. Inhomogeneous Transport: Compensating the Source Error Term

The compensation of $\mathcal{O}(\delta t)$ truncation error in (25) dependent on the advective fluxes of the source term is important for preserving the global accuracy and stability of forward-in-time (FT) approximations (20) [25, 28]. This particular error term appears in those “naive” approximations to (19) that simply combine an FT advection scheme for homogeneous transport with an $\mathcal{O}(\delta t^2)$ approximation of $R^{n+1/2}$. Ignoring this error leads to spurious $\sim \mathcal{O}(\delta t)$ sinks/sources of “energy” Ψ^2 and, eventually, to nonlinear instability (Appendix A in [28]). Compensating this error to $\mathcal{O}(\delta t^2)$ only requires subtracting a first-order-accurate approximation from the RHS of (20). This can be further upgraded and/or simplified depending upon a particular approximation adopted for representing $R^{n+1/2}$ in (20). We discuss below two important cases.

⁶ For a discussion of some formal issues at $\Psi \rightarrow 0$ see Section 3.2 in [23].

First we assume that $R^{n+1/2}$ can be written as $0.5(R^n + R^{n+1})$, where R^{n+1} is an $\mathcal{O}(\delta t^2)$ accurate approximation to R at $t = (n + 1)\delta t$. Then a simple, efficient, and fully second-order accurate MPDATA realization of (20) can be compactly written as

$$\Psi_{\mathbf{i}}^{n+1} = \text{MPDATA}(\Psi^n + 0.5\delta t R^n, \mathbf{V}^{n+1/2}, G) + 0.5\delta t R_{\mathbf{i}}^{n+1}. \quad (32)$$

In the above equation, MPDATA symbolizes the homogeneous-transport algorithm discussed in Section 3.2. Advecting the auxiliary field $\Psi^n + 0.5\delta t R^n$ not only compensates the truncation error due to the source term but it also has the physical interpretation of integrating the forces along a parcel trajectory rather than at the grid point. This makes (32) congruent to semi-Lagrangian approximations (see Section 2 in [28]) and facilitates unified fluid models that integrate the equations of motion, optionally, in the Eulerian (point-wise) or Lagrangian (trajectory-wise) sense [31]. Note that (32) may be viewed as a paraphrase of the Strang splitting [34].

Second we consider the alternate case, where $R^{n+1/2}$ is already a known $\mathcal{O}(\delta t^2)$ approximation to R at $t = (n + 1/2)\delta t$. Then, a fully second-order scheme for (19) can be written as

$$\Psi_{\mathbf{i}}^{n+1} = \text{MPDATA}(\Psi^n, \mathbf{V}^{n+1/2}, G) + \text{MPDATA}^*(R^{n+1/2}, 0.5\mathbf{V}^{n+1/2}, G), \quad (33)$$

where both MPDATAs refer to the homogeneous-transport algorithms in Section 3.2. Note that MPDATA* may use different options than MPDATA. In particular, for overall second-order accuracy it can be the cheapest $IORD = 1$ (i.e., donor cell) scheme. Note also that in a computer program the two terms in (32) or (33) may be evaluated separately at several distinct stages (see Section 4 for examples).

3.4. Approximating the Advective Velocities

Estimating the advective velocity in (20) at the intermediate $n + 1/2$ time level results in cancellation of the $\sim \Delta t(\partial \mathbf{v}/\partial t)$ truncation errors in (25). Temporal staggering of the advective velocity may be approximated by linear interpolation or extrapolation

$$\mathbf{v}^{n+1/2} = \frac{1}{2}(\mathbf{v}^{n+1} + \mathbf{v}^n), \quad \mathbf{v}^{n+1/2} = \frac{1}{2}(3\mathbf{v}^n - \mathbf{v}^{n-1}), \quad (34a), (34b)$$

either of which maintains second-order accuracy in (32) or (33). The linearity of the approximations in (34) is advantageous in anelastic systems, where it ensures $\nabla \cdot \mathbf{v}^{n+1/2} = 0$ (given $\nabla \cdot \mathbf{v}^n = 0 \forall n$). Formula (34a) is an obvious choice in hybrid models [23], where the momenta are integrated with centered-in-time-and-space schemes and the thermodynamic variables employ FT approximations. Then evaluation of the velocities prior to the thermodynamic variables ensures the availability of \mathbf{v}^{n+1} in (34a). One advantage of (34a) is that it does not affect computational stability [28]. The approximation (34b) is a natural choice in models where all variables are evaluated with FT transport algorithms. Compared to (34a), the theoretical disadvantages of (34b) are: increased memory requirement, a larger amplitude of the truncation error, and a more restrictive stability condition—(34b) may require half of the time-step allowed in (34a) [28]. In practice, (34a) and (34b) offer similar overall accuracy in hybrid anelastic models [23], while satisfactory performance of (34b) in the fully FT fluid models has been documented in [25] and [31] for the elastic and anelastic models, respectively.

The stability of FT approximations (20) for elastic fluids may be augmented using a nonlinear extrapolation consistent with the Lagrangian counterpart of (19) for momenta

$$\tilde{\mathbf{v}}^{n+1/2} = \tilde{\mathbf{v}}^n - \dot{\mathbf{x}}^n \cdot \nabla \tilde{\mathbf{v}}^n \frac{\Delta t}{2} + \tilde{\mathbf{R}}^n \frac{\Delta t}{2}, \quad (35)$$

where $\tilde{\mathbf{v}}$ is the specific momentum with the corresponding forcing $\tilde{\mathbf{R}}$, and the convective term employs a first-order-accurate upwind differencing for the spatial discretization [28]. Although neither $\tilde{\mathbf{v}}$ nor $\tilde{\mathbf{R}}$ may appear explicitly in (19), they are both known functionals of the dependent variables. An $\mathcal{O}(\delta t^2)$ approximation to $\mathbf{V}^{n+1/2}$ in (32) or (33) can be readily recovered from (35). In elastic FT models, (35) allows a time-step up to four times larger than does (34b) [28].

3.5. Other Options

The options discussed so far are the most elementary. Other options may further enhance the overall accuracy, reduce computational costs, or simplify the coding. The MPDATA literature contains numerous discussions of additional degrees of freedom. Here we draw the reader's attention to a few of these.

(1) *“Third-order-accurate” scheme.* The analysis in Sections 2.1 and 2.2 can be repeated using a third-order Taylor series expansion that leads to a positive definite and third-order-accurate advection algorithm for the constant coefficient case [13]. For variable flows and $G \neq 1$ in (19), the scheme is only second-order accurate with its leading error proportional to the second derivatives of the transporting velocities and G . Its primary advantage is a more uniform distribution of the truncation error as a function of the Courant number [13]. At a given resolution, this preserves better the solution symmetries and benefits problems dependent on passive scalar advection such as pollutant transport in smooth flows. This option complicates the $IORD = 3$ basic scheme substantially. For a 3D flow $\mathbf{v} = (u, v, w)$ in an $\mathbf{x} = (x, y, z)$ framework, the “third-order” corrections to the pseudo velocities in (29) are straightforward finite difference approximations to expressions like

$$\begin{aligned} \delta U = & \frac{\delta x^2}{6} \left(\frac{3U|U|}{G} - \frac{2U^3}{G^2} - U \right) \frac{1}{\Psi} \frac{\partial^2 \Psi}{\partial x^2} + \frac{\delta x \delta y V}{2G} \left(|U| - \frac{2U^2}{G} \right) \frac{1}{\Psi} \frac{\partial^2 \Psi}{\partial x \partial y} \\ & + \frac{\delta x \delta z W}{2G} \left(|U| - \frac{2U^2}{G} \right) \frac{1}{\Psi} \frac{\partial^2 \Psi}{\partial x \partial z} - \frac{2\delta y \delta z UVW}{3G^2} \frac{1}{\Psi} \frac{\partial^2 \Psi}{\partial y \partial z}, \end{aligned} \quad (36)$$

where U, V, W denote respective local Courant numbers $V^l \delta t / \delta x^l$. The remaining two components (δV and δW) of the “third-order” correction are obtained by the symmetric permutation.

(2) *Recursive pseudo velocities.* As more elaborate features are incorporated into MPDATA, the formulae for the pseudo velocities become more complicated, and the resulting schemes become computationally more intensive. MPDATA options such as, for example, a monotonicity-preserving third-order-accurate scheme may benefit from yet another degree of freedom. Instead of repeating successive MPDATA iterations, one may consider an alternate scheme that employs the two-pass scheme with the pseudo velocity derived assuming the summation of an infinite number of MPDATA iterations [13]; see Fig. 1d, for illustration. Although this special recursive pseudo velocity itself is quite complicated

and does not benefit simple MPDATA schemes, it can offer savings up to 50% when combined with other options. Also the recursive velocities provide an efficient option for those programs whose architecture penalizes numerous passes.

(3) *Nonoscillatory option.* The algorithm in (26)–(30) preserves sign but not monotonicity of the transported variables [22–24] and, in general, the solutions are not free of spurious extrema. In most cases preservation of sign is adequate [26]. When required, MPDATA can be made fully monotone [24] by employing FCT formalism [37] to limit the pseudo velocities. In fact, MPDATA is very well suited for this for a number of reasons. First, the initial MPDATA iteration is the donor cell scheme—a low-order monotone scheme commonly used as the reference in the FCT design. Second, assuring monotonicity of subsequent iterations provides a higher-order accurate reference solution for the next iteration with the effect of improving the overall accuracy of the resulting FCT scheme. Third, since all MPDATA iterations have similar low phase errors characteristic of the donor cell scheme [23], the FCT procedure mixes solutions with consistent phase errors. This benefits significantly the overall accuracy of the resulting FCT scheme (see Fig. 5 in [24] and the accompanying discussion).

(4) *Diffusion.* The simulation of diffusive transport illustrates especially well the flexibility of the MPDATA approach. In particular it shows that, from the viewpoint of finite difference approximation, the distinction between advection and forcing in (19) may be arbitrary. Consider a special case of (19), where $R \equiv \nabla \cdot (K \nabla \Psi)$. The resulting advection–diffusion problem can be integrated to the second-order using algorithms (32) or (33) with R^{n+1} or $R^{n+1/2}$ denoting suitable first-order-accurate estimates.⁷ An alternate option draws from the underlying idea of the basic MPDATA itself, i.e., the formal equivalence between the diffusion and advection equations on a discrete mesh (section 3.2 in [23]). The diffusive flux may be formally written in a form of advective flux $K \nabla \Psi \equiv -\Omega \Psi$, where $\Omega = -(K/\Psi) \nabla \Psi$ (if $\Psi \neq 0$; $\Omega = 0$ otherwise). Adding a first-order-accurate estimate for $\Omega^{n+1/2}$ to the advective velocity $\mathbf{V}^{(1)}$ in (28b) transforms the advection–diffusion problem into a simple MPDATA advection.

In geophysical applications, where flows exhibit large Reynolds’ numbers, the diffusion terms are typically evaluated to first-order. This is justified because significant diffusion enters the equations of motion only as a consequence of subgrid-scale turbulence models, where the diffusivity $K \sim \mathcal{O}(\delta x^l)$. This eliminates the need for a predictor step— $\text{as } R^{n+1/2} \approx R^{n+1} \approx R^n$ and $\Omega^{n+1/2} \approx \Omega^n \approx \Omega^{n+1}$, both with accuracy to $\mathcal{O}(\delta t)$ —and opens new possibilities for further simplifications (see Section 4.2 for an example).

4. EXAMPLES OF APPLICATIONS

Here we supplement the theory of the preceding sections with two examples. These illustrate designs of FT finite difference fluid models (20) based solely on the MPDATA approach for both elastic and anelastic systems with, respectively, explicit and implicit (in time) approximations of the pressure forces. The first problem, a shallow-fluid flow on a rotating sphere, has been proposed in [36] for evaluating the accuracy and efficiency of numerical methods for global scale dynamics and has become a benchmark in the field.

⁷ Although (32) could be used with implicit methods for diffusive fluxes, here we emphasize the explicit diffusion schemes typical of geophysical models.

Its solution evolves through coupling of wave propagation and material motions leading to some steepening of planetary waves, but otherwise remains smooth. The second problem is a benchmark from the area of small scale dynamics—large eddy simulation (LES) of convective planetary boundary layer [14], complicated by the addition of topography. In contrast to the first problem, here the flow is fully 3D and turbulent. For finite difference FT methods the issues to address are the accurate time-centering of the pressure-gradient and inertial forces, proper incorporation of the metric terms, and minimization of diffusive errors. Inadequate treatment of the forces and metric terms can be a source of unphysical oscillations or even lead to computational instability [28]. Excessive numerical diffusion will prevent the steepening of the wave in the first problem and will result in unphysical turbulence spectra in the second.

4.1. Shallow Fluid on the Sphere

The equations expressing conservation of mass and momentum in a shallow fluid flow on a rotating sphere (cf. section 2.6 in [36]) each has the form of the generalized transport equation (19)

$$\frac{\partial G\Phi}{\partial t} + \nabla \cdot (\mathbf{v}\Phi) = 0, \quad (37a)$$

$$\frac{\partial GQ_x}{\partial t} + \nabla \cdot (\mathbf{v}Q_x) = GR_x, \quad (37b)$$

$$\frac{\partial GQ_y}{\partial t} + \nabla \cdot (\mathbf{v}Q_y) = GR_y, \quad (37c)$$

where $G \equiv h_x h_y$ (with h_x and h_y representing the metric coefficients of the general orthogonal coordinates (x, y)), and $\Phi \equiv H - H_o$ is the depth of the fluid (with H and H_o denoting the heights of the free surface and the bottom, respectively). $\mathbf{Q} \equiv (\Phi \dot{x} h_x, \Phi \dot{y} h_y)$ is the momentum vector with corresponding forcings⁸

$$R_x = -\frac{g}{h_x} \Phi \frac{\partial(\Phi + H_o)}{\partial x} + f Q_y + \frac{1}{G\Phi} \left(Q_y \frac{\partial h_y}{\partial x} - Q_x \frac{\partial h_x}{\partial y} \right) Q_y, \quad (38a)$$

$$R_y = -\frac{g}{h_y} \Phi \frac{\partial(\Phi + H_o)}{\partial y} - f Q_x - \frac{1}{G\Phi} \left(Q_y \frac{\partial h_y}{\partial x} - Q_x \frac{\partial h_x}{\partial y} \right) Q_x. \quad (38b)$$

Here g is the acceleration of gravity and f is the Coriolis parameter. The Lagrangian counterpart of (37), employed for predicting advective velocities via (35), reduces to

$$\frac{D\tilde{\mathbf{v}}}{Dt} \equiv \left(\frac{\partial}{\partial t} + \dot{\mathbf{x}} \cdot \nabla \right) \tilde{\mathbf{v}} = \tilde{\mathbf{R}}, \quad (39)$$

where $\tilde{\mathbf{v}} = (1/\Phi)\mathbf{Q}$, and $\tilde{\mathbf{R}} = (1/\Phi)\mathbf{R}$. The advective velocity \mathbf{v} and the specific momentum $\tilde{\mathbf{v}}$ are related through $\mathbf{v} = (\tilde{v}_x h_y, \tilde{v}_y h_x)$.

The integration of the discrete equations over a time-step using the model algorithm (32) proceeds in four distinct steps. First, the advective Courant numbers at the $n + 1/2$ time

⁸ In contrast to a common approach for high-speed flows, it is not advantageous to include pressure in the momentum flux.

level are computed using appropriate fields at the n time level in (35). Second, the first term on the RHS of (32) is evaluated for the mass and momentum fields. Third, the new values of the pressure forces are recovered from the updated depth. At this stage the only unknown elements required to solve (32) are the inertial forces (second and third terms on the RHS of (38)) at the $n + 1$ time level. An updated solution for the momentum within a cell may be compactly written as

$$\mathbf{Q} = \mathbf{Q}^* + \frac{1}{2}\Delta t\mathcal{F}(\mathbf{Q}), \quad (40)$$

where \mathbf{Q} refers to $n + 1$ time level, \mathbf{Q}^* denotes all known terms [i.e., the first term on the RHS of (32), plus half of the new pressure force], and $\mathcal{F}(\mathbf{Q})$ represents the inertial part of the forces in (38). The simple implicit vector formula (40) is solved by means of successive iterations with one iteration sufficing for a second-order-accurate solution (Section 4 in [28]). The implicit character of (40) is dictated not by stability, but rather by accuracy and computational efficiency.

For illustration, we simulate the evolution of a Rossby–Haurwitz wave described in [36]. The current experimental setup assumes in (37)–(39) the spherical coordinates $x = \lambda$, $y = \theta$, $h_x = a \cos \theta$, and $h_y = a$, where λ , θ , and a denote longitude, latitude, and the sphere’s radius, respectively. The uniform, unstaggered mesh⁹ consists of 128 points in longitude, and 64 points in latitude. The time-step is limited by the propagation speed of the gravity wave [28]; see [16] for optional designs relaxing the stability condition. Figure 2a shows the initial condition. Over several days, we expect this initial pattern to move from west to east with little change of shape (expect for a slight steepening of the wave in mid-latitudes) and angular velocity $\sim 2.5 \times 10^{-6}$ rad s⁻¹ [36]. Figure 2b shows the numerical solution after 5 days of integration using the linearized MPDATA for divergent flows (Section 3.2.3 and 3.2.4; for an equivalent solution using basic MPDATA for divergent flows see Section 4 in [28]). This solution is in good agreement with theoretical estimates (0.34 π displacement after 5 days and ~ 100 ms⁻¹ maximal velocity of the flow), as well as with predictions of a spectral model [8, 11].

4.2. Convective Boundary Layer over a Steep Hill

The nonhydrostatic anelastic model used in this section has been described in [31]. Here, we consider a stratified nonrotating fluid whose undisturbed (hydrostatic ambient) state is described by the profiles of the potential temperature and the velocity: $\Theta_e = \Theta_e(z_C)$, and $\mathbf{v}_e = \mathbf{v}_e(z_C)$, respectively (recall that the subscript C refers to Cartesian coordinates). The standard terrain-following system of coordinates $[x, y, z] = [x_C, y_C, H(z_C - h)/(H - h)]$ assumes a model depth H and an irregular lower boundary $h = h(x_C, y_C)$. The coordinate transformation enters the governing equation of motion through the coefficients of the metric tensor $G^{IJ} = (\partial x^I/\partial x_C^K)(\partial x^J/\partial x_C^K)$, and the Jacobian of transformation $G = \text{Det}\{\partial \mathbf{x}_C/\partial \mathbf{x}\} = (\text{Det}\{G^{IJ}\})^{-1/2}$.

Given the assumptions above, the anelastic conservation laws for momentum and entropy may be written in the form resembling (19),

$$\frac{\partial \rho^* \Psi}{\partial t} + \nabla \cdot (\mathbf{v}^* \Psi) = \rho^* F^\Psi + \rho^* \mathcal{D}^\Psi, \quad (41)$$

⁹ Note that on an unstaggered grid (40) is fully local and so it can be solved individually, cell by cell.

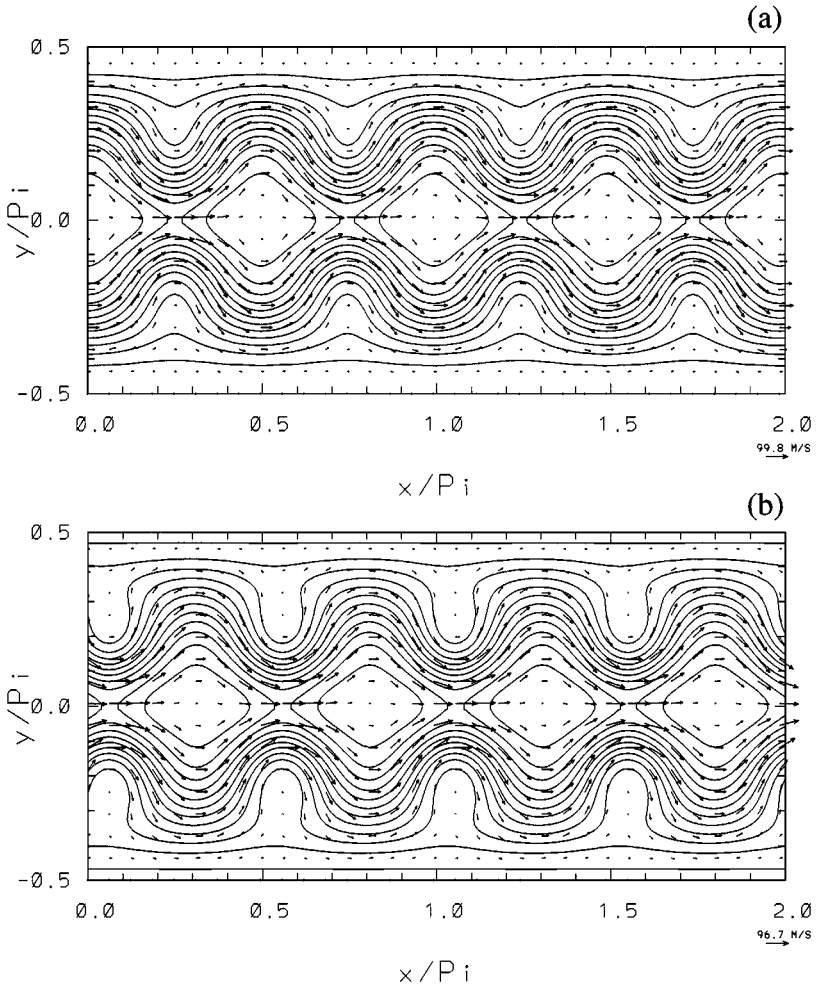


FIG. 2. Geopotential perturbation ($H/\bar{H} - 1$, where $\bar{H} = 8$ km) and the flow vectors for the Rossby–Haurwitz wave test problem: (a), the initial condition; (b), numerical solution after 5 days using a second-order accurate MPDATA scheme. The contour interval is 0.05.

where Ψ denotes any of the three Cartesian velocity components (u, v, w) or the potential temperature Θ , and $\rho^* \equiv \bar{\rho}G$ with $\bar{\rho} = \bar{\rho}(z_C)$ denoting the reference “Boussinesq” density (cf. [15]). The advective velocity $\mathbf{v}^* \equiv \rho^*(u, v, w)$ satisfies the anelastic mass conservation law,

$$\frac{\partial \bar{\rho}Gu}{\partial x} + \frac{\partial \bar{\rho}Gv}{\partial y} + \frac{\partial \bar{\rho}G\omega}{\partial z} = \nabla \cdot \mathbf{v}^* = 0, \tag{42}$$

where $\omega \equiv \dot{z}$ is the “vertical” component of transformed (contravariant) velocity related to the Cartesian (covariant) velocity components through

$$\omega = G^{-1}w + G^{13}u + G^{23}v. \tag{43}$$

The associated F^Ψ and D^Ψ terms on the RHS of (41) represent, respectively, the resolved

and subgrid-scale part of the total forcings. The subgrid-scale terms are fairly complex but standard—their explicit form is unimportant for the current discussion. Here, we employ a turbulence model based on the prognostic turbulent kinetic energy (TKE) equation following [19]. The resolved forcings take the explicit form

$$F^u \equiv -\frac{\partial\phi}{\partial x} - G^{13}\frac{\partial\phi}{\partial z} - \alpha(u - u_e), \quad F^v \equiv -\frac{\partial\phi}{\partial y} - G^{23}\frac{\partial\phi}{\partial z} - \alpha(v - v_e) \quad (44a), (44b)$$

$$F^w \equiv -\frac{\partial\phi}{\partial z} + g(\Theta - \Theta_e)/\overline{\Theta} - \alpha(w - w_e), \quad F^\Theta \equiv -\alpha'(\Theta - \Theta_e). \quad (44c), (44d)$$

Here ϕ is the pressure perturbation with respect to the undisturbed environmental profile normalized by $\bar{\rho}$. The potential temperature $\Theta = \overline{\Theta}(z_C)$, in the denominator of the buoyancy term in (44c), refers to the reference state. The attenuation forcings absorb gravity waves in the vicinity of the open boundaries of the model.

The integration of the discrete equations over a time-step uses (32) on a regular un-staggered mesh. It proceeds in several distinct steps. First, the advective Courant numbers at the $n + 1/2$ time level are computed using (34b). Second, the first term on the RHS of (32) is evaluated for u , v , w , and Θ fields. This is also a convenient stage to update the TKE variable ($e \equiv \sqrt{TKE}$ in our case), which takes a particularly simple form $e^{n+1} = \text{MPDATA}(e^n + \delta t R^e |^n, \mathbf{V}^{n+1/2}, G)$ as the subgrid-scale physics is approximated only to the first-order (Section 3.5.4). In the third step, the vector of preliminary values of dependent variables generated in the preceding step is projected onto solenoidal flows [4]. This requires a straightforward algebraic inversion of the implicit system composed of four equations (32), and the formulation of the boundary value problem for pressure ϕ^{n+1} implied by the continuity constraint (42) and the relation (43). The resulting elliptic equation is solved (subject to appropriate boundary conditions) using the generalized conjugate-residual approach (see [29–31] for further details). Having advanced all model variables in time, the last step evaluates all forcings required in the second step of the next cycle.

For illustration, we highlight the results of large-eddy simulation of the convective boundary layer past a steep hill—an extension of a standard problem in Cartesian geometry [14]. The specific model setups are similar to those in [32]. We assume a Boussinesq fluid ($\overline{\rho}_{,z_C} = \overline{\Theta}_{,z_C} = 0$) with $\mathbf{v}_e = 0$; $\Theta_e = \overline{\Theta}$ for $z_C \leq 500$ m and increases linearly aloft. A uniform heat flux is imposed along the surface of an axially symmetric steep cosine hill (Figs. 3a and b). The mesh consists of $N_x \times N_y \times N_z = 65 \times 65 \times 51$ grid points with $\delta x = \delta y = 50$ m and $\delta z = 30$ m. The time step $\delta t = 10$ s results in maximal Courant number $\lesssim 1$ throughout the entire integration ($N_t = 1500$ time steps). The boundary conditions are periodic in x and y and rigid in z (a weak gravity-wave absorber is employed near the upper boundary).

Figure 3a shows a vertical cross section through the normalized subgrid-scale viscosity field $K' = K_{TKE}\delta t(\delta x^2 + \delta y^2 + \delta z^2)^{-1}$, at $T = N_t\delta t$ when the boundary layer is well developed. In the reference run with flat lower boundary (not shown), the model reproduces the standard results [14]. Figure 3b shows horizontal cross sections of w field at $z_C = 360\text{m} = 0.52z_i$, where z_i is the height of the boundary layer in the reference run at this same time. Finally, Fig. 3c, shows the power spectra of w for the current and the reference runs. the influence of the hill on the shape of the boundary layer (Fig. 3a), on the formation of coherent structures (Fig. 3b), as well as on the selection of scales (Fig. 3c) is apparent.

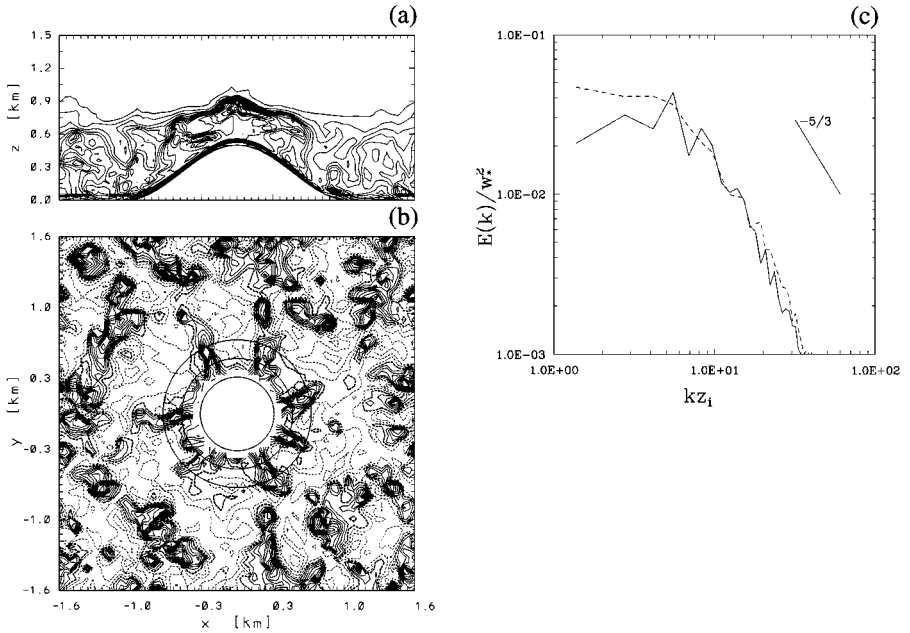


FIG. 3. Large-eddy simulation of convective boundary layer over a steep hill. Plate (a) shows vertical, center section through the field of normalized subgrid-scale viscosity with the field's maximum, minimum, and contour interval equal 2.4×10^{-3} , 2.4×10^{-4} , and 1.2×10^{-4} , respectively. Plate (b) shows horizontal cross section through the field of vertical velocity at $z_c = 360$ m with the field's maximum, minimum, and contour interval equal, respectively, 1.5, -0.5 , and 0.125 ms^{-1} . Plate (c) shows the spectra of the resolved vertical velocity fluctuations at $z_c = 360$ m for the current simulation (solid line) and the reference run over flat boundary (dashed line).

The simulations reported employed classical MPDATA for solenoidal flows (Section 3.2.2) and its linearized variant (Section 3.2.4), respectively, for Θ and momenta; both schemes incorporated the nonoscillatory option (Section 3.5.3).

ACKNOWLEDGMENTS

We thank Vanda Grubišić, Robert Sharman, and Zbigniew Sorbjan for their assistance in developing the subgrid-scale turbulence program used in Section 4.2. We are grateful to William Anderson for his help with graphics. Since 1991, our work on MPDATA has been supported in part by the Department of Energy "Computer Hardware, Advanced Mathematics, Model Physics" (CHAMMP) research program.

REFERENCES

1. W. D. Anderson and P. K. Smolarkiewicz, A comparison of high performance Fortran and message passing parallelization of a geophysical fluid model, in *Parallel Computational Fluid Dynamics: Algorithms and Results Using Advanced Computers*, edited by P. Shiano, A. Ecer, J. Periaux, and N. Satofuka (Elsevier Science, Amsterdam, 1997), p. 384.
2. W. D. Anderson, V. Grubišić, and P. K. Smolarkiewicz, Performance of a massively parallel 3D non-hydrostatic atmospheric fluid model, in *Proceedings of the International Conference on Parallel and Distributed Processing Techniques and Applications, PDPTA '97, Las Vegas, Nevada, June 30–July 3*, edited by H. R. Arabnia (CSREA, 1997), p. 645.

3. C. W. Beason and L. G. Margolin, *DPDC: A Second-Order Monotone Scheme for Advection*, Lawrence Livermore National Laboratory, Report UCRL-99731, p. 11 (1988).
4. A. J. Chorin, Numerical solution of the Navier–Stokes equations, *Math. Comp.* **22**, 742 (1968).
5. H. Drange and R. Bleck, Multidimensional forward-in-time and upstream-in-space-based differencing for fluids, *Mon. Wea. Rev.* **125**, 616 (1997).
6. S. K. Godunov, A difference scheme for numerical computation of discontinuous solutions of equations in fluid dynamics, *Math. Sb.* **47**, 271 (1959).
7. W. W. Grabowski and P. K. Smolarkiewicz, Monotone finite-difference approximations to the advection-condensation problem, *Mon. Wea. Rev.* **118**, 2082 (1990).
8. J. J. Hack and R. Jakob, *Description of a Global Shallow Water Model Based on the Spectral Transform Method*, National Center for Atmospheric Research, Technical Note No. NCAR/TN-343+STR, p. 39 (1992).
9. A. Harten, B. Engquist, S. Osher, and S. R. Chakravarthy, Uniformly high-order accurate essentially non-oscillatory schemes III, *J. Comput. Phys.* **71**, 231 (1987).
10. W. Hecht, W. R. Holland, and P. J. Rasch, Upwind-weighted advection schemes for ocean tracer transport: An evaluation in a passive tracer context, *J. Geophys. Res.* **100**, 20763 (1995).
11. R. Jakob, J. J. Hack, and D. Williamson, *Solutions to the Shallow Water Test Set Using the Spectral Transform Method*, National Center for Atmospheric Research, Technical Note No. NCAR/TN-388+STR, p. 82 (1993).
12. C. E. Leith and L. G. Margolin, *Turbulence modeling in the SHALE code*, Lawrence Livermore National Laboratory, Report UCRL-ID-103271, p. 30 (1990).
13. L. G. Margolin and P. K. Smolarkiewicz, *Antidiffusive Velocities for Multipass Donor Cell Advection*, *SIAM J. Sci. Comput.*, to appear (1998); extended version available as Lawrence Livermore National Laboratory report # **UCID-21866**, p. 44 (1989).
14. F. T. M. Nieuwstadt, P. J. Mason, C-H Moeng, and U. Schumann, Large-eddy simulation of convective boundary-layer: A comparison of four computer codes, in *Turbulent Shear Flows 8*, edited by H. Durst et al. (Springer-Verlag, New York/Berlin, 1992), p. 343.
15. J. M. Prusa, P. K. Smolarkiewicz, and R. R. Garcia, On the propagation and breaking at high altitudes of gravity waves excited by tropospheric forcing, *J. Atmos. Sci.* **53**, 2186 (1996).
16. J. M. Reisner, L. G. Margolin, and P. K. Smolarkiewicz, A reduced grid model for shallow flows on the sphere, in *Parallel Computational Fluid Dynamics: Implementations and Results Using Parallel Computers*, edited by A. Ecer, J. Periaux, N. Satofuka, and S. Taylor (Elsevier Science, 1996), p. 537.
17. P. J. Roache, *Computational Fluid Dynamics* (Hermosa, Albuquerque, NM, 1972).
18. C. Schär and P. K. Smolarkiewicz, A synchronous and iterative flux-correction formalism for coupled transport equations, *J. Comput. Phys.* **128**, 101 (1996).
19. U. Schumann, Subgrid length-scales for large-eddy simulation of stratified turbulence, *Theoret. Comput. Fluid Dynamics* **2**, 279 (1991).
20. A. P. Siebesma and coauthors, Intercomparison of 3D/2D cloud resolving models and 1D parameterizations for the shallow-cumulus topped boundary layer, *Bound.-Layer Meteor.*, in preparation (1998).
21. P. K. Smolarkiewicz, A simple positive definite advection scheme with small implicit diffusion, *Mon. Wea. Rev.* **111**, 479 (1983).
22. P. K. Smolarkiewicz, A fully multidimensional positive definite advection transport algorithm with small implicit diffusion, *J. Comput. Phys.* **54**, 325 (1984).
23. P. K. Smolarkiewicz and T. L. Clark, The multidimensional positive definite advection transport algorithm: Further development and applications, *J. Comput. Phys.* **67**, 396 (1986).
24. P. K. Smolarkiewicz and W. W. Grabowski, The multidimensional positive definite advection transport algorithm: Nonoscillatory option, *J. Comput. Phys.* **86**, 355 (1990).
25. P. K. Smolarkiewicz, On forward-in-time differencing for fluids, *Mon. Wea. Rev.* **119**, 2505 (1991).
26. P. K. Smolarkiewicz, Nonoscillatory advection schemes, in *Numerical Methods in Atmospheric Models, Proceedings of Seminar on Numerical Methods in Atmospheric Models, ECMWF, Reading, UK, 9–13 September 1991*, p. 235.
27. P. K. Smolarkiewicz and G. A. Grell, A class of monotone interpolation schemes, *J. Comput. Phys.* **101**, 431 (1992).

28. P. K. Smolarkiewicz and L. G. Margolin, On forward-in-time differencing for fluids: Extension to a curvilinear framework, *Mon. Wea. Rev.* **121**, 1847 (1993).
29. P. K. Smolarkiewicz and L. G. Margolin, Variational solver for elliptic problems in atmospheric flows, *Appl. Math. & Comp. Sci.* **4**, 527 (1994).
30. P. K. Smolarkiewicz, V. Grubišić, and L. G. Margolin, On forward-in-time differencing for fluids: Stopping criteria for iterative solutions of anelastic pressure equations, *Mon. Wea. Rev.* **125**, 647 (1997).
31. P. K. Smolarkiewicz and L. G. Margolin, On forward-in-time differencing for fluids: An Eulerian/semi-Lagrangian nonhydrostatic model for stratified flows, in *Numerical Methods in Atmospheric and Oceanic Modelling. The André Robert Memorial Volume*, edited by C. Lin, R. Laprise, and H. Ritchie (Canadian Meteorological and Oceanographical Society, Ottawa, Canada, 1997), p. 127. [Companion volume to *Atmosphere-Ocean*]
32. Z. Sorbjan, Numerical study of penetrative and 'solid lid' nonpenetrative convective boundary layers, *J. Atmos. Sci.* **53**, 101 (1996).
33. D. E. Stevens and S. Bretherton, A forward-in-time advection scheme and adaptive multilevel flow solver for nearly incompressible atmospheric flow, *J. Comput. Phys.* **129**, 283 (1996).
34. G. Strang, On the construction and comparison of difference schemes, *SIAM J. Numer. Anal.* **5**, 506 (1968).
35. P. K. Sweby, High resolution schemes using flux limiters for hyperbolic conservation laws, *SIAM J. Numer. Anal.* **21**, 995 (1984).
36. D. L. Williamson, J. B. Drake, J. J. Hack, R. Jakob, and P. N. Swarztrauber, 1992, A standard test set for numerical approximations to the shallow water equations on the sphere, *J. Comput. Phys.* **102**, 211 (1992).
37. S. T. Zalesak, Fully multidimensional flux-corrected transport algorithms for fluids, *J. Comput. Phys.* **31**, 335 (1979).